frontiers in Materials

ORIGINAL RESEARCH
published: 14 February 2019
doi: 10.3389/fmats.2019.00009

The Effect of Blast Furnace Slag/Fly Ash Ratio on Setting, Strength, and Shrinkage of Alkali-Activated Pastes and Concretes

Abeer M. Humad[1,2]*, *Ankit Kothari*[1], *John L. Provis*[3] and *Andrzej Cwirzen*[1]

[1] Structural Engineering Division, Luleå University of Technology, Luleå, Sweden, [2] Civil Engineering Department, Babylon University, Hillah, Iraq, [3] Department of Materials Science and Engineering, University of Sheffield, Sheffield, United Kingdom

The aim of this study was to determine the effects of partial fly ash substitution in to a series of alkali-activated concrete based on a high-MgO blast furnace slag BFS. Mixes were activated with various amounts of sodium silicate at alkali modulus (mass ratio SiO_2/Na_2O) values of 1.0, 0.5, and 0.25. The results showed that, an increase in the fly ash content extended the initial setting time but had very little effect on the final setting time, although the early age compressive strength was decreased. The fly ash addition had no effect on the drying shrinkage but lowered the autogenous shrinkage. The mixes activated with sodium silicate at a lower alkali modulus showed a significantly higher autogenous shrinkage but lower drying shrinkage values. Severe micro cracking of the binder matrix was observed only for mixes without fly ash, activated with sodium silicate solution at higher alkali modulus. Decreasing the alkali modulus resulted in a higher autogenous shrinkage, less micro cracking and a more homogenous structure due to more extensive formation of sodium-aluminate-silicate-hydrate gel (N-A-S-H), promoted by the addition, and more extensive reaction of the fly ash.

Keywords: fly ash FA, blast furnace slag BFS, initial and final setting time, shrinkage, alkali-activated binders

OPEN ACCESS

Edited by:
Carlos Chastre, Faculdade de Ciências e Tecnologia da Universidade Nova de Lisboa, Portugal

Reviewed by:
Ionut Ovidiu Toma, Gheorghe Asachi Technical University of Iaşi, Romania
Yonghao Fang, Hohai University, China
Marcello Romagnoli, University of Modena, Italy; Reggio Emilia, Italy

***Correspondence:**
Abeer M. Humad
abeer.humad@ltu.se; abeer_alasady@yahoo.com

Specialty section:
This article was submitted to Structural Materials, a section of the journal Frontiers in Materials

Received: *17 September 2018*
Accepted: *24 January 2019*
Published: *14 February 2019*

Citation:
Humad AM, Kothari A, Provis JL and Cwirzen A (2019) The Effect of Blast Furnace Slag/Fly Ash Ratio on Setting, Strength, and Shrinkage of Alkali-Activated Pastes and Concretes. Front. Mater. 6:9. doi: 10.3389/fmats.2019.00009

INTRODUCTION

Alkali activated cementitious binders (AAB) have been intensively studied over the last few decades (Collins and Sanjayan, 1999; Duxson et al., 2007; Chi et al., 2012; Provis and van Deventer, 2014; Liu et al., 2016). AABs are based on aluminosilicate industrial by-products and natural resources, e.g., fly ash (FA), ground granulated blast furnace slag (BFS), metakaolin or rice husk ash, activated by a source of alkalis. The properties of concretes made with AAB depend on the type, the amount and the concentration of the alkaline solution used for their activation, the curing temperature and the precursor type (Bernal et al., 2014; Jang et al., 2014). The chemical activator is usually, an alkaline solution of soluble hydroxides, alkali silicates or carbonates. Relatively high calcium content is often associated with the formation of an Al-substituted C-S-H (C-(A)-S-H) gel (Wang and Scrivener, 1995; Myers et al., 2015). Generally, the structure of the C-(N)-A-S-H phase is similar to the C-S-H phase formed in Portland cement based system but with a lower calcium content (Shi et al., 2006; Myers et al., 2013). The main reaction product of alkali-activated fly ash is a N-A-S-H gel (Na_2O-Al_2O_3-SiO_2-H_2O) with a three-dimensional (Q^4) framework of tetrahedral SiO_4 and AlO_4 linked through shared oxygen atoms (Škvára et al., 2003; Provis, 2014; Walkley et al., 2018) and with a low bound water content. The activation of fly ash requires pH $\geq$13 to take place (Bijen, 1996).

The production of alkali activated binders based on a combination of BFS and FA has become popular, as provides an opportunity to tailor binder formulation to offset some of the observed difficulties in AAB formulation, which can including for example; delayed setting time, large shrinkage, requirement for heat curing, insufficient workability, or slow strength development (Smith and Osborne, 1977; Oh et al., 2010; Bernal et al., 2013; Gao et al., 2015; Marjanović et al., 2015; Keulen et al., 2018).

In the case of blast furnace slag-fly ash blended systems the reaction rate generally increases with higher amounts of slag and at higher activator amounts, but this can come at the cost of more challenging workability including relatively rapid slump loss (Bijen, 1996; Nath and Sarker, 2014; Provis and van Deventer, 2014). An increased amount of fly ash delayed the setting, reduced the compressive strength, modulus of elasticity and Poisson's ratio and resulted in high ductility and toughness (Škvára et al., 2003; Lee and Lee, 2013; Nath and Sarker, 2014; Criado et al., 2016; Liu et al., 2016) but enhanced the homogeneity of the hardened matrix and limited the microcracking (Wardhono et al., 2015). The addition of a naphthalene-based superplasticizer appeared to have very little effect on the initial and on the final setting times while a polycarboxylate-based superplasticizer showed an accelerating effect (Jang et al., 2014). Increasing the BFS content decreased the slump of a fresh mix (Nath and Sarker, 2014).

Increasing the amount of alkaline solution up to a certain limit, does increase the compressive strength (Nath and Sarker, 2014; Humad et al., 2018). The pore size distribution of the alkali-activated fly ash/slag systems tended to be finer in comparison with hydrated Portland cement (Collins and Sanjayan, 2000; Lee and Lee, 2013; Provis and van Deventer, 2014). Broadly, the development of early-age strength is associated with the reaction of BFS, while later strength gains come from the effect of the fly ash.

The main reaction product of the BFS/FA system has been identified to be the a mixture of C–A–S–H gel and N–A–S–H gel (Ismail et al., 2014; Lee et al., 2014), and this gives the chance to generate a binder matrix which is denser and less porous than those of the pure BFS-based or FA-based binders due to the increased reactivity of the blended precursors and formation of both C-A-S-H and N-A-S-H type gels in stable coexistence (Jang et al., 2014; Lee et al., 2014; Lee and Lee, 2015; Criado et al., 2016).

Blast furnace slags rich in magnesia are common in several countries, including for example Sweden (Humad et al., 2018), but are not very widely studied in the context of alkali-activation; data related to fresh concrete characteristics, shrinkage and creep are very sparse. Alkali activation of these slags, e.g., by sodium silicate tends to form a C-A-S-H type gel as the main binding phase, and a hydrotalcite-like Mg-Al layered double hydroxide as a secondary product (Richardson et al., 1994; Bernal, 2016). The incorporation of Al in the C-A-S-H tends to decrease with increasing MgO content as more hydrotalcite forms, and no substitution of Ca by Mg in the C-A-S-H was detected even at high MgO content (Ben Haha et al., 2011).

Alkali activated binder (AAB) concretes have been observed to show high autogenous shrinkage, attributed to a fine pore structure leading to a high tensile stress at the water to air meniscus interface (Ma and Dehn, 2017). Autogenous shrinkage can occur also in the hardened stat due to self-desiccation in small pores (Holt, 2001). However, previous research has shown no direct relation between the shrinkage and the mass loss in the AAB (Samson et al., 2017). The autogenous and the drying shrinkage tended to increase with a higher amount of slag in a BFS/FA (Zheng, 2009; Lee et al., 2014; Deb et al., 2015). However, both the ultimate autogenous and the ultimate drying shrinkage tended to be higher in comparison with concrete based on Portland cement due to increased volume of mesopores (Cartwright et al., 2014; Lee et al., 2014; Ma and Dehn, 2017).

The research presented in this publication is focused on AABs produced from MgO-rich slags, and effects of fly ash and alkali activator on fresh and hardened concrete properties. A special emphasis placed on understanding the relationship between phase composition, shrinkage and microcracking of the binder matrix.

MATERIALS AND METHODS

A ground granulated blast furnace slag (BFS), type Merit 5000 (MEROX-Sweden) and fly ash (FA) provided by Heidelberg Cement (Cementa-Sweden), were used, in ratios (BFS:FA) of 100:0, 80:20, 60:40, 50:50, and 40:60. The chemical compositions and some physical properties of the precursors are shown in **Table 1**.

The mix proportions of the pastes and concretes studied are shown in **Tables 2**, **3**, respectively. All mixes contain 450 kg/m^3 of binder and the w/b ratio was 0.45 for concrete 0.36 for pastes. Liquid sodium silicate (SS) provided by PQ Corporation had an alkali modulus (M_s = mass ratio SiO_2/Na_2O) of = 2.2, with 34.37 wt.% SiO_2, 15.6 wt.% Na_2O and a solids content of 49.97 wt.%. The mixes were activated by SS solutions having M_s values of 0.25, 0.5, and 1.0, adjusted by the addition of sodium hydroxide

TABLE 1 | Chemical composition and physical properties of BFS and fly ash used in this work, measured by X-ray fluorescence, and represented as oxides.

Oxide	CaO	SiO_2	Al_2O_3	Fe_2O_3	MgO	Na_2O	K_2O	TiO_2	MnO	P_2O_5	SO_3	LOI
BFS wt.%	30.4	35	14.3	0.3	16.1	0.6	0.7	2.8	0.5	–	0.7	0.9
Fly ash wt.%	6.1	48.1	18.9	7.8	1.8	1.1	2.3	0.8	0.073	0.44	–	1.6
Physical data	**Specific surface cm^2/g**				**Bulk density kg/m^3**				**Particle density kg/m^3**			
BFS	5,000				1,100				2,950			
Fly ash	3,200				1,000				2,300			

TABLE 2 | Mix proportions of pastes.

Mix ID	Slag: fly ash ratio	Water/binder ratio	Wt.% of sodium silicate (SS) as soild content	Alkali modulus (M_S)	pH of the alkali solution after 1 h
100:0-5SS1	100:0	0.36	5%	1	**13.5**
80:20-5SS1	80:20		5%	1	
60:40-5SS1	60:40		5%	1	
50:50-5SS1	50:50		5%	1	
40:60-5SS1	40:60		5%	1	
100:0-10SS1	**100:0**	**0.36**	**10%**	**1**	**13.7**
80:20-10SS1	**80:20**		**10%**	**1**	
60:40-10SS1	**60:40**		**10%**	**1**	
50:50-10SS1	**50:50**		**10%**	**1**	
40:60-10SS1	**40:60**		**10%**	**1**	
100:0-10SS0.5	100:0	0.36	10%	0.5	**14**
80:20-10SS0.5	80:20		10%	0.5	
60:40-10SS0.5	60:40		10%	0.5	
50:50-10SS0.5	50:50		10%	0.5	
40:60-10SS0.5	40:60		10%	0.5	
100:0-10SS0.25	**100:0**	**0.36**	**10%**	**0.25**	**14**
80:20-10SS0.25	**80:20**		**10%**	**0.25**	
60:40-10SS0.25	**60:40**		**10%**	**0.25**	
50:50-10SS0.25	**50:50**		**10%**	**0.25**	
40:60-10SS0.25	**40:60**		**10%**	**0.25**	
100:0-14SS1	100:0	0.36	14%	1	**13.7**
80:20-14SS1	80:20		14%	1	
60:40-14SS1	60:40		14%	1	
50:50-14SS1	50:50		14%	1	
40:60-14SS1	**40:60**		**14%**	**1**	

pellets (98% purity) to the stock solutions. The alkali activator dosages used were 5, 10, and 14 wt.% of the binder amount as a solid content. The aggregate content was 1,662 kg/m^3. Coarse and fine aggregates were provided by Jehander Heidelberg Cement group, Sweden, and had a specific gravity of 2.7 t/m^3.

The liquid sodium silicate was pre-mixed with water either 1 or 24 h before casting. The different pre-mixing times were related the distribution of the experimental work over a longer period. Control measurement showed that pH values for both activators different by <0.1 pH units in every case between activators tested after 1 and 24 h. Activators prepared 1 h before mixing were used for pastes used for measure initial and final setting times, for the XRD analysis and for preliminary concretes mixes to determine the 7-day compressive strength test, **Tables 2**, **3**. Activators prepared 24 h before the mixing were used to produce concrete samples utilized to determine 7- and 28-day compressive strength values, **Figure 6**, shrinkage, **Figures 7**, **8**, and for the SEM-BSE study, **Figure 9**.

The mixing procedure included mixing of all dry ingredients for 1 min followed by the addition of all mixing water with the alkali activator and mixing for another 3 min. Concrete samples for preliminary work (7-day compressive strength) were produced using the Hobart mixer model A200N. Concretes specimens (for main work) of shrinkage, compressive strength were produced using a rotating pan mixer type Zyklos-ZZ75HE.

Initial and final setting times were determined following the ASTM C191-13 (ASTM C191-13, 2013) standard using the Vicat apparatus. The slump was determined following the ASTM C143 (ASTM C143/C143M-15a, 2015) standard. The pH values of the activator solution were determined as an average of three measurements of the using ORION STAR A211 pH meter produced by Thermo SCIENTIFIC. The compressive strength specimens had dimensions of 100 × 100 × 100 mm^3. Three cubes were tested for the 7- and 28- day age following the SS-EN 12390-3 standard. Immediately after casting, all samples were tightly sealed with plastic foil and cured at 20 ± 2°C and 42 ± 2% RH until testing. The compressive strength machine produced by Toni Technik, Berlin—Germany was used, and the load rate was kept constant at 10 kN/s. XRD analysis was done on 28-day old powdered paste samples using a PANanalytical Empyrean XRD unit operating with Cu Kα radiation. The total scanning time for each sample was 15 min and the step size was 0.0262° 2O. A scanning electron microscopy (SEM) JSM-IT100, was used to study the microstructure of hardened samples with a QUANTAX energy dispersive X-ray spectrometer (EDX)-analysis system from Bruker, using the ESPRIT 2 software. Concrete samples for SEM studies were impregnated with resin and polished. Autogenous and drying shrinkage strains were measured with an electronic manual strain gauge DEMEC type (Mayes Instruments). Two cylinder specimens with a diameter of 100 mm and height of 200 mm were used for each test. Three pairs of stainless steel studs were glued on each concrete cylinder. Specimens for the determination of the autogenous shrinkage were sealed using a plastic foil while specimens for the determination of the drying shrinkage were exposed unprotected to laboratory conditions 20 ± 2°C and 42 ± 2% RH.

THE TEST RESULTS AND DISCUSSION

The combined effects of M_s and of the amount of the FA on the recorded initial and final setting times of AAB pastes are shown in

TABLE 3 | Mix properties of concretes.

Mix ID	BFS: FA ratio	binder content kg/m^3	$\frac{w}{b}$ ratio	wt.% SS as solid content	Alkali modulus Ms	Fine agg. content (0–4 mm) kg/m^3	Coarse agg. content (4–8 mm) kg/m^3	pH of the alkali solution after 24 h
MAIN MIXES								
100:0-10SS 1	100:0	450	0.45	10%	1			13.8
80:20-10SS 1	80:20				1			13.8
80:20-10SS 0.5	80:20				0.5	1,247	415	14
PRELIMINARY MIXES FOR 7-DAY COMPRESSIVE STRENGTH TESTING								pH of the alkali solution after 1 h
80:20-5SS1	80:20	450	0.45	5%	1	1,247	415	13.5
60:40-5SS1	60:40	450	0.45	5%	1	1,247	415	
50:50-5SS1	50:50	450	0.45	5%	1	1,247	415	
40:60-5SS1	40:60	450	0.45	5%	1	1,247	415	
80:20-10SS1	80:20	450	0.45	10%	1			13.7
80:20-10SS0.5					0.5			14
80:20-10SS0.25					0.25	1,247	415	14
60:40-10SS1	60:40	450	0.45	10%	1			13.7
60:40-10SS0.5					0.5			14
60:40-10SS0.25					0.25	1,247	415	14
50:50-10SS1	50:50	450	0.45	10%	1			13.7
50:50-10SS0.5					0.5	1,247	415	14
50:50-10SS0.25					0.25			14
40:60-10SS1	40:60	450	0.45	10%	1			13.7
40:60-10SS0.5					0.5			14
40:60-10SS0.25					0.25	1,247	415	14
80:20-14SS1	80:20	450	0.45	14%	1	1,247	415	13.7
60:40-14SS1	60:40	450	0.45	14%	1	1,247	415	
50:50-14SS1	50:50	450	0.45	14%	1	1,247	415	
40:60-14SS1	40:60	450	0.45	14%	1	1,247	415	

Figures 1A,B. The amount of SS was held constant at 10 wt.% (as a solid content) of the total binder content for all these samples. The initial setting time was not significantly affected by BFS replacements of up to 50 wt.%. However, 60 wt.% replacement of BFS by FA caused a delay of the initial setting time by nearly 350 min for the mix activated with SS having at $M_s = 0.5$. At $M_s = 0.25$, fly ash incorporation gives a delay in what would otherwise have been an inconveniently rapid initial set, and at 60% FA the retardation is sufficient to bring the setting time into the rang of setting time values required by standard such as EN 197-1 or ASTM C1157, which do not allow initial setting time shorter than 45 min for common cement. The final setting time was affected only to a limited extent by fly ash incorporation, **Figure 1B**, in agreement with earlier (Chang, 2003). The lag between the initial and final setting time was quite long in all instances, with some mixes demonstrating both an initial set that was too fast under ASTM C1157 (requiring initial set $\geq$45 min), and a final set that was too slow for the requirements of the same standard (final set in $\leq$ 420 min). No direct relation between the alkali modulus M_s (1 and 0.5) and the initial setting time was identified, but decreasing the M_s to 0.25 showed a reduction in the initial setting time. The initial and final setting times were not strongly correlated across all mixes tested. However, the strongest delay of the setting time due to FA addition occurred at $M_s = 1$, **Figure 1**, which was also observed by others (Chang, 2003; Lee and Lee, 2013).

The effects of FA on the initial and final setting time were more pronounced for mixes containing a lower dose (5 wt.%) of the alkali activator, **Figures 2A,B**. In the case of the mix containing 60 wt.% FA and activated with 5 wt.% SS at $M_s = 1$, the delay of the initial setting time was nearly 850 min, compared to 300 min at 20 wt.% FA. This is related to the significantly lower initial reactivity of the fly ash than BFS at ambient temperature, and the need for a pH $\geq$13 for fly ash to react at a meaningful rate (Bijen, 1996; Sakai et al., 2005; Lee and Lee, 2013; Nath and Sarker, 2014). **Figure 3** presents the correlation between the alkali modulus M_s and pH values of the sodium silicate solutions used to give 10 wt.% activator doses as a solid content. This shows that as the activator begins to react with BFS and its dissolved silicate precipitations in to the first C-A-S-H to form; its pH will be likely to increase as its effective M_s decreases. Therefore, the presence of a large quantity of BFS supplying calcium to react with silicate from the activator will potentially bring a more rapid increase in the pH, which means that the fly ash reaction is initiated sooner, and the delay from its addition is less extensive. The high MgO content of BFS is unlikely to contribute very significantly to this aspect of the reaction mechanism, beyond depolymerizing the slag glass as a network modifier, as it reacts predominantly with

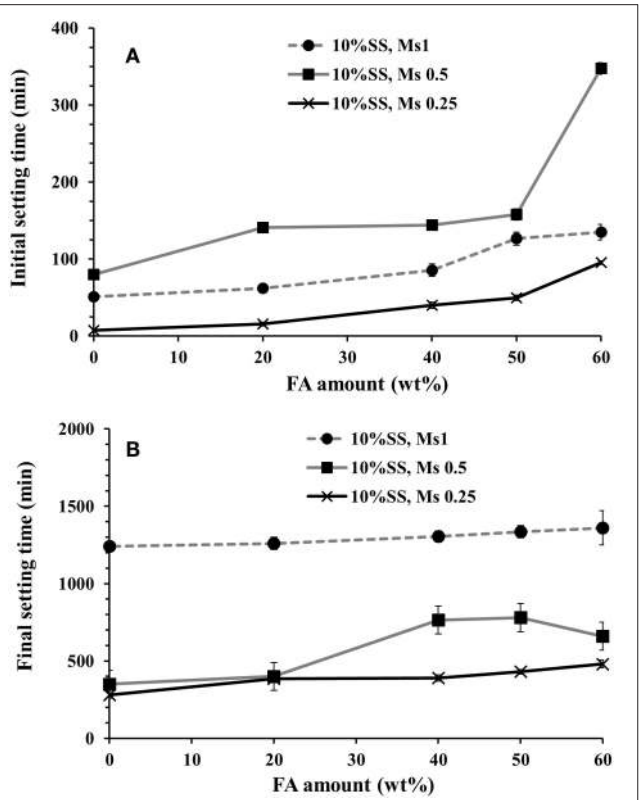

FIGURE 1 | (A) Initial setting times, **(B)** final setting times of pastes activated with 10 wt.% sodium silicate (SS) and different alkali modulus M_S.

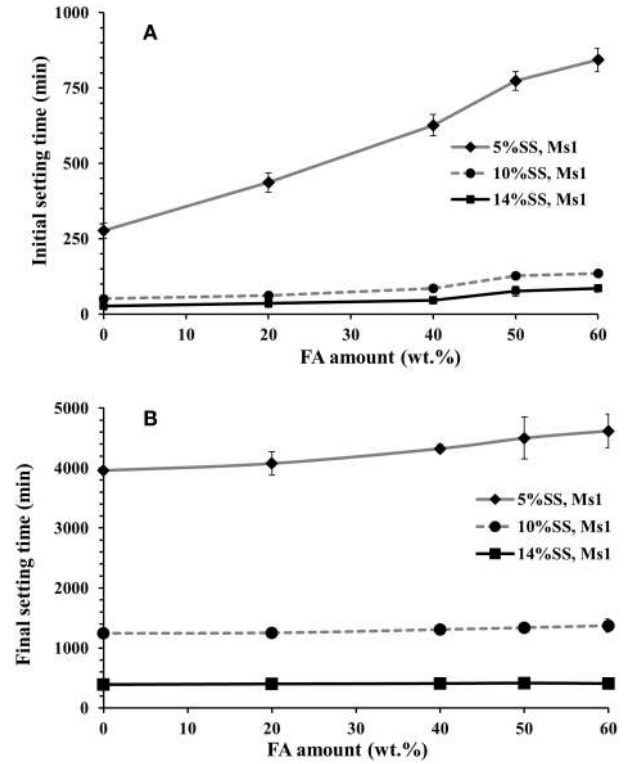

FIGURE 2 | (A) Initial setting times and **(B)** final setting times of pastes activated with different doses of sodium silicate (SS) with alkali modulus $M_S = 1$.

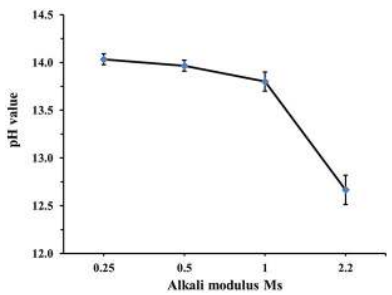

FIGURE 3 | Relationship between the alkali modulus M_S and pH value of the sodium silicate solution used to give 10 wt.% activator doses (as solid content). measured after 1 h of mixing.

Al and so does not compete with (or act in synergy with) the Ca in removing Si from solution.

Compressive strength values determined after 7 days of curing, for concretes based on these pastes, show a general decrease with increasing FA addition, **Figures 4**, **5**. The dose of the sodium silicate, which varied between 5 and 14 wt.% (as solid content) at constant M_s of 1, for these samples did not have a strong effect when FA was present, **Figure 4**.

Interestingly, nearly the same 7-day compressive strength values were obtained for mixes containing various amounts of FA and activated with 5 and 10 wt.% SS, **Figure 4**. The 7-day compressive strength values were significantly more affected by the alkali modulus (M_s) when the amount of the FA was increased, **Figure 5**. The lowest strength were recorded for mixes activated at $M_s = 1.0$, and the highest for $M_s = 0.5$ and 0.25, which is in line with earlier results (Zheng, 2009; Mosale Vijayakumar, 2014). Reducing the M_s from one to 0.5 doubled the 7-days compressive strength value due to increase of the alkalinity of the solution, which in turn increased the dissolution rate of the solid precursor particles. On the contrary, no significant change of the 7 days compressive strength values was observed when the M_s decreased from 0.5 to 0.25, **Figure 5**. The mixing procedure included mixing of all dry ingredients for 1 min followed by the addition of all mixing water with the alkali activator and mixing for another 3 min.

The 28-day compressive strengths were studied for three concrete mixes (100:0-10SS1, 80:20-10SS1, and 80:20-10SS0.5), **Figure 6**. As mentioned earlier, these mixes were activated with the SS solution produced 24 h prior to the casting, **Table 3** (main mixes). While all other mixes (preliminary mixes) used alkali activator solutions prepared just 1 h before the mixing, **Figures 4**, **5**. Even though the difference in pH measurement of activator solutions of pre-mixed 1 and 24 h was <0.1, the main mixes for 7- and 28-day, autogenous and drying shrinkage tests were pre-mixed 1 day before to see if there is any effect on gaining strength. The effects of the preparation of alkali activators on their efficiency were studied earlier by Hardjito and

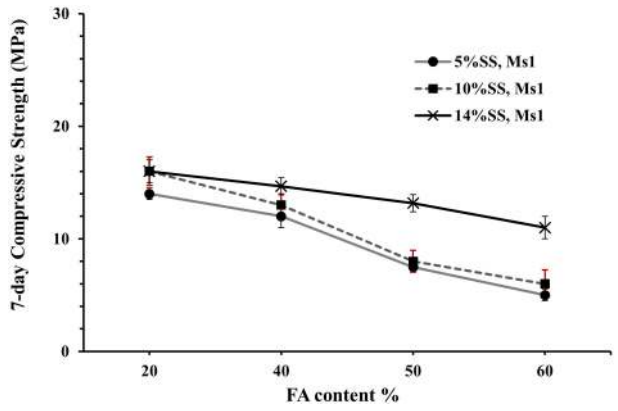

FIGURE 4 | Effect of adding fly ash on 7-day compressive strength for AASF concrete cubes activated by different doses of sodium silicate as marked, with alkali modulus 1.

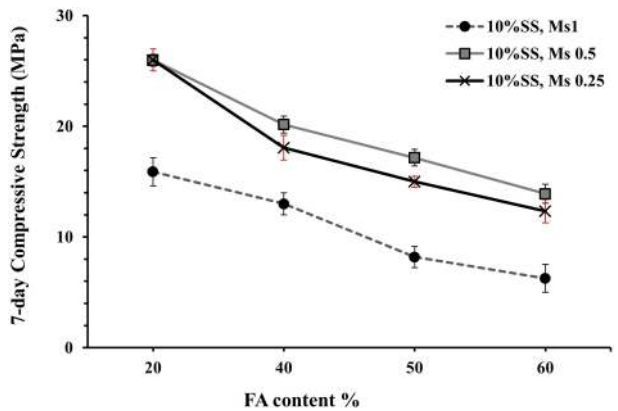

FIGURE 5 | Effect of adding fly ash on 7-day compressive strength for AASF concrete cubes activated by 10 wt.%SS with different alkali modulus values as marked.

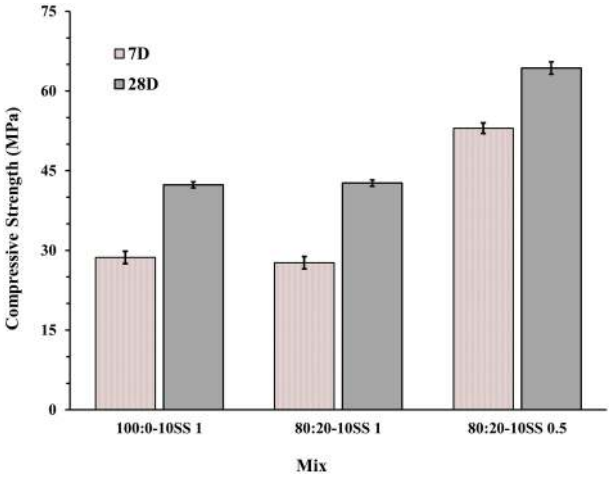

FIGURE 6 | Seven and twenty-eight days compressive strength results for concrete cubes of main mixes.

Rangan (2005), where established that 24 h earlier preparation of activator presented higher strength values. The results in this study showed that pre-mixing of the activator solution 24 h before casting and using the pan mixer increased the early compressive strength, in spite of the quite small differences in pH values (Yang and Jennings, 1995; Hardjito and Rangan, 2005). The replacement of 20 wt.% of the BFS with FA did not significantly lower neither the 7- nor 28-days compressive strength values. The decreased alkali modulus M_s from 1 to 0.5 doubled the strength. It can be directly related to a higher alkalinity of the mix with a lower M_s and thus to a higher reactivity of the precursor (Cartwright et al., 2014; Singh et al., 2016; Humad et al., 2018). Earlier studies also showed that the optimum alkali modulus M_s was in the range between 1.0–1.5 for basic slags, 0.9–1.3 for neutral, and 0.75–1.25 for acid slags (Bakharev et al., 1999; Mithun and Narasimhan, 2014). However, Fernandez and Palomo observed that increasing the concentration of the Na_2O, by decreasing the M_s value lead to stronger condensation and to an increased strengths (Fernández-Jiménez and Palomo, 2005). In the present study, the addition of the fly ash to the high MgO activated slag produced the highest strength values at a low $M_s = 0.5$.

Drying and autogenous shrinkage were determined for three concrete mixes containing 80 wt.% BFS and 20 wt.% FA, and activated with 10 wt.% dosage of SS solution at M_s of either 1.0 or 0.5, **Figures 7**, **8**. Additionally, a reference concrete mix (mix 100:0-10SS1) containing only BFS activated by 10 wt.% SS at $M_s = 1.0$ was casted, **Table 3** (main mixes). In general, and contrary to some published criticisms of concrete based on AABs, the total measured shrinkage value was similar to or even lower than the shrinkage usually measured in concretes based on Portland cement according to the literatures (Zhang et al., 2013; Cartwright et al., 2014; Niknezhad et al., 2017). The results showed no significant effect of replacing FA-BFS replacement on the drying shrinkage of concretes activated by 10 wt.% SS having $M_s = 1$, **Figure 8**. Decreasing M_s to 0.5 caused a significant reduction in the drying shrinkage, but conversely, the autogenous shrinkage values were increased. This may be related to the higher pH of the pore solution, which led to more extensive chemical reactions to form hydrate products at lower M_s. The formation of finer microstructure in combination with a more intensive self-desiccation is thus identified to have caused the increased autogenous shrinkage, while the higher strength of the concrete at $M_s = 0.5$ provides it with more ability to resist stresses induced by drying forces (and restrained by the aggregate) after hardening, and thus to show lower shrinkage.

The analysis of the chemical composition of hardened matrixes was conducted using the combination of XRD and SEM-EDS. The XRD test results for pastes are shown in **Figure 9**. The FA contained crystalline quartz, mullite, hematite and maghemite, and an amorphous phase. The BFS showed only amorphous (glassy) material. Hardened pastes showed the presence of C-A-S-H and N-A-S-H in mixes have FA. Earlier studies have shown that the N-A-S-H type gels are very likely to

coexist with C-A-S-H type gels across much of the compositional range of alkali-activated blast furnace slags in blends with fly ash (Garcia-Lodeiro et al., 2011; Bernal et al., 2013). The hydrotalcite related peaks were observed in pastes containing up 20 wt.% FA which is in agreement with previous studies of high MgO content BFS (Bernal et al., 2014).

The SEM-BSE study revealed microcracking of the binder matrix of mixes containing 100% BFS (mix 100:0-10SS1), **Figure 10**. Micro-cracks formed in the bulk binder matrix and in the interfacial transition zone (ITZ); these may have formed in part due to vacuum treatment of the samples for loading into the SEM, but are also consistent with the relative degrees of drying shrinkage observed in the concrete samples, and so are primarily attributed to that process. Conversely, no cracking was observed in either of the mixes containing 20 wt.% FA, 80:20-10SS1 and 80:20-10SS 0.5. Reduced microcracking in the case of 80:20-10SS 0.5 can potentially be related to the observation of higher tensile strength of the binder matrix and lower shrinkage values, **Figures 7**, **8**, but neither of these characteristics are evident for 80:20-10SS1 compared to 100:0-10SS1, so it is also likely that the chemical nature of the gels (and particularly the degree of binding of water) is important in determining microcracking potential. The involvement of fly ash in the reaction process is expected to yield a binder containing more N-A-S-H phases, which intrinsically bind less water than C-A-S-H, and so react differently under exposure to drying conditions. The type of gel formed is influenced by the Ca + Mg content, the Si/Al ratio in the reactive binder component, and the alkalinity of the activating solution (Provis, 2014). The SEM-BSE images of the concrete samples here show the presence of several constituents binder, remnant BFS and FA, and aggregates distinguished by different gray levels related to variation in average atomic number density, **Figure 10**. EDX spot analysis was performed in a number of points in the binder matrix to determine the amounts of SiO2, CaO, and Al_2O_3 as shown in the form of the pseudo ternary diagram (normalized by content of these oxides, i.e., neglecting any other constituents) in **Figure 11**. The binder regions in all of the concrete samples showed elemental compositions consistent with the joint formation of N-A-S-H and C-A-S-H phases, lying in between the chemical composition of pure forms of each of these phases, and consistent with the literature for AABs based on BFS with and without FA inclusion.

However, the relative amount of each phase was influenced by the presence of the FA and the alkali modulus of the sodium silicate activator (Myers et al., 2013; Ismail et al., 2014). The concrete containing 20 wt.% FA activated with $M_s = 1$ showed C-(A)-S-H gel and more of the N-A-S-H than the binder with no FA. The 20 wt.% FA mix activated with $M_s = 0.5$ showed even more dominance of the N-A-S-H gel, consistent with the discussion above regarding a higher degree of reaction of the FA with this activator. Similar trends were also observed in concretes

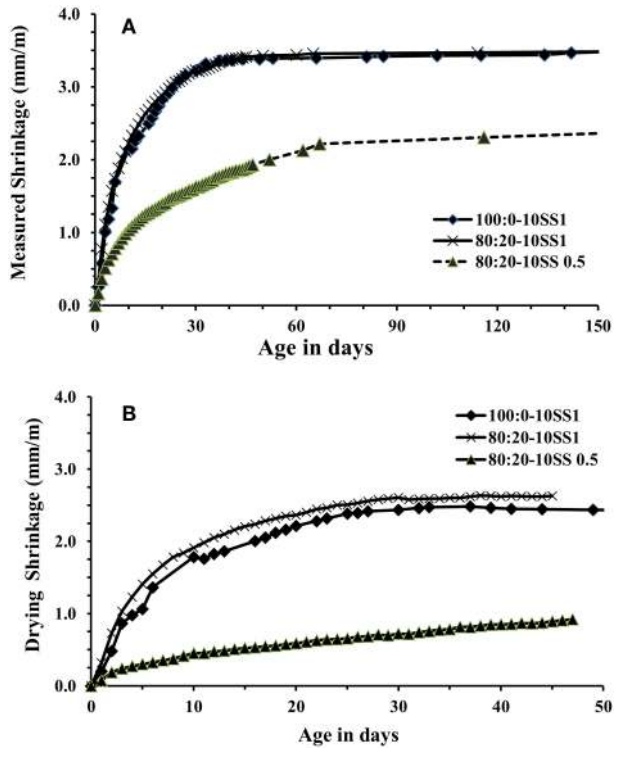

FIGURE 7 | Drying shrinkage results of concrete cylinders in laboratory environment (20 ± 2°C and 42 ± 2%RH), **(A)** Total measured shrinkage, **(B)** drying shrinkage.

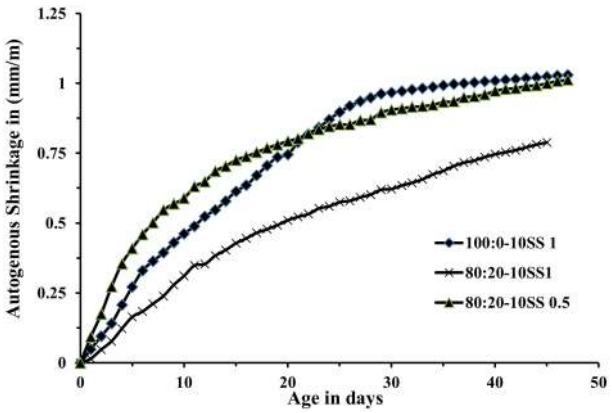

FIGURE 8 | Autogenous shrinkage (sealed) of concrete cylinder specimens in laboratory environment (20 ± 2°C and 42 ± 2% RH).

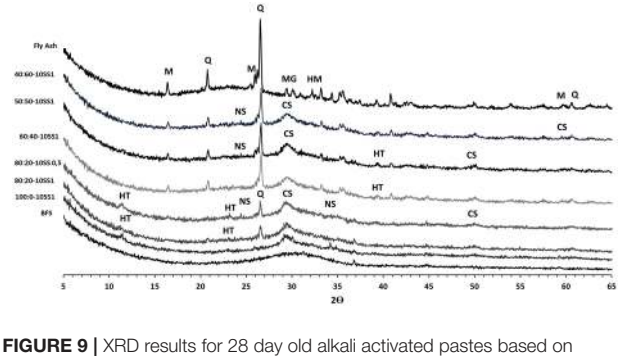

FIGURE 9 | XRD results for 28 day old alkali activated pastes based on BFS/FA activated with 10%SS and data for anhydrous slag and fly ash for comparison. Q, quartz; M, mullite; HM, hematite; MG, maghemite; CS, C-A-S-H; HT, hydrotalcite; NS, N-A-S-H.

based on BFS sources with a more moderate MgO content, and in related binder system (Kumar et al., 2010; Garcia-Lodeiro et al., 2011; Provis, 2014).

Numerical data from the EDX analysis, expressed as SiO_2, Al_2O_3 and CaO content are summarized in **Figure 11**. Addition of 20 wt.% FA to the mix and lowering the alkali modulus was consistent with the presence of more N-A-S-H phases. According to the calculated phase diagrams for alkali-activated BFS-based binder (Myers et al., 2017), a high MgO content slag tends to form C-A-S-H and hydrotalcite more than N-A-S-H, but the results presented here show that this trend could be reversed by the presence of the FA as this supplies a large amount of extra Al into the chemical reaction process of binder formation.

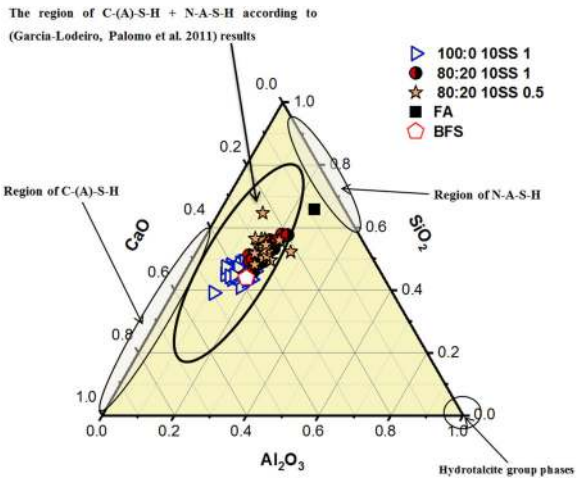

FIGURE 11 | Ternary diagram showing the oxides component ranges in the mixes, and the formation regions of different gels according to the literature.

CONCLUSIONS

The addition of fly ash influenced both fresh and hardened binder matrix properties of cements based on alkali activated

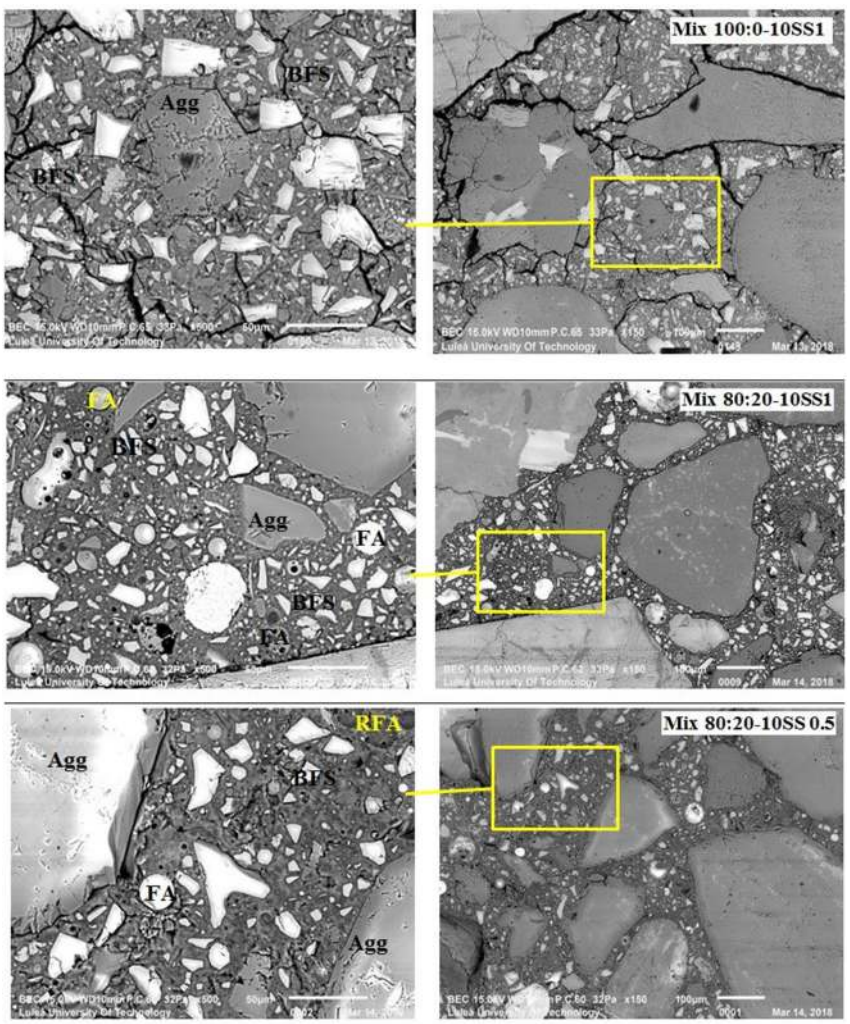

FIGURE 10 | SEM-BSE images of 1 year old concrete samples. FA, Unreacted or partially reacted fly ash particle; BFS, Unreacted or partially reacted blast furnace slag particle; RFA, full reacted Fly ash particle; Agg, aggregate particle.

high-MgO blast furnace slag. Increasing the fly ash content delayed the initial setting time but had little effect on the final setting time, although the lag from initial to final setting remained much longer than is normal for Portland cement. Pre-mixing the activator solution 24 h before increased the 7- and 28-days compressive strength, even despite negligible changes in pH. Fly ash addition reduced the 7-days compressive strength but showed significant enhancement when used in a concrete activated by sodium silicate at a lower alkali modulus (i.e., at $M_s = 0.5$ or $M_s = 0.25$). Fly ash had no significant effect on the drying shrinkage, but substantially lowered the autogenous shrinkage. Decreasing the alkali modulus M_s from one to 0.5 nearly doubled the 7-days compressive strength of all mixes containing FA. The use of an alkali activator with a lower alkali modulus caused a higher autogenous shrinkage. The fly ash significantly limited the microcracking of the binder matrix. All these effects were related to the phase composition of the hardened binder matrix the addition of the fly ash promoted the formation of additional N-A-S-H gel along with the C-A-S-H and hydrotalcite formed by the reaction of the blast furnace slag. The presence of this additional N-A-S-H gel was associated with a stronger and less micro crack-prone binder matrix.

AUTHOR CONTRIBUTIONS

AH: organized the database, performed the statistical analysis and wrote the first draft of the manuscript. AK: organized some of the database, performed some of the statistical analysis. JP and AC: revision, read and approved the submitted version.

FUNDING

This work was supported by Ministry of Higher Education and Scientific Research - Iraq and Luleå University of Technology (LTU) – Sweden.

ACKNOWLEDGMENTS

We would like to thank the The Iraqi Ministry of Higher Education and Scientific Research, Iraq and Technical Staff of the Laboratory at LTU, Sweden.

REFERENCES

ASTM C143/C143M-15a (2015). Standard Test Method for Slump of Hydraulic-Cement Concrete, West Conshohocken, PA: *ASTM International*.

ASTM C191-13 (2013). Standard Test Methods for Time of Setting of Hydraulic Cement by Vicat Needle, West Conshohocken, PA: ASTM International.

Bakharev, T., Sanjayan, J. G., and Cheng, Y. (1999). Alkali activation of australian slag cements. *Cement Concrete Res.* 29, 113–120. doi: 10.1016/S0008-8846(98)00170-7

Ben Haha, M., Lothenbach, B., Le Saout, G., and Winnefeld, F. (2011). Influence of slag chemistry on the hydration of alkali-activated blast-furnace slag—Part I: effect of MgO. *Cement Concrete Res.* 41, 955–963. doi: 10.1016/j.cemconres.2011.05.002

Bernal, S. A. (2016). Advances in near-neutral salts activation of blast furnace slags. *RILEM Tech. Lett.* 1, 39–44. doi: 10.21809/rilemtechlett.2016.8

Bernal, S. A., Provis, J. L., Walkley, B., San Nicolas, R., Gehman, J. D., Brice, D. G., et al. (2013). Gel nanostructure in alkali-activated binders based on slag and fly ash, and effects of accelerated carbonation. *Cement Concrete Res.* 53, 127–144. doi: 10.1016/j.cemconres.2013.06.007

Bernal, S. A., San Nicolas, R., Myers, R. J., De Gutiérrez, R. M., Puertas, F., Van Deventer, J. S., et al. (2014). MgO content of slag controls phase evolution and structural changes induced by accelerated carbonation in alkali-activated binders. *Cement Concrete Res.* 57, 33–43. doi: 10.1016/j.cemconres.2013.12.003

Bijen, J. (1996). Benefits of slag and fly ash. *Construct. Building Mat.* 10. 309–314. doi: 10.1016/0950-0618(95)00014-3

Cartwright, C., Rajabipour, F., and Radlinska, A. (2014). Shrinkage characteristics of alkali-activated slag cements. *J. Mat. Civ. Eng.* 27:B4014007. doi: 10.1061/(ASCE)MT.1943-5533.0001058

Chang, J. (2003). A study on the setting characteristics of sodium silicate-activated slag pastes. *Cement Concrete Res.* 33, 1005–1011. doi: 10.1016/S0008-8846(02)01096-7

Chi, M., Chan, g., and Huang, R. (2012). Strength and drying shrinkage of alkali-activated slag paste and mortar. *Adv. Civil Eng.* 2012:579732. doi: 10.1155/2012/579732

Collins, F., and Sanjayan, J. (1999). Workability and mechanical properties of alkali activated slag concrete. *Cement Concrete Res.* 29. 455–458. doi: 10.1016/S0008-8846(98)00236-1

Collins, F., and Sanjayan, J. (2000). Effect of pore size distribution on drying shrinking of alkali-activated slag concrete. *Cement Concrete Res.* 30, 1401–1406. doi: 10.1016/S0008-8846(00)00327-6

Criado, M., Aperador, W., and Sobrados, I. (2016). Microstructural and mechanical properties of alkali activated Colombian raw materials. *Materials* 9:158. doi: 10.3390/ma9030158

Deb, P. S., Nath, P., and Sarker, P. K. (2015). Drying shrinkage of slag blended fly ash geopolymer concrete cured at room temperature. *Proc. Eng.* 125, 594–600. doi: 10.1016/j.proeng.2015.11.066

Duxson, P., Provis, J. L., Lukey, G. C., and Van Deventer, J. S. (2007). The role of inorganic polymer technology in the development of 'green concrete'. *Cement Concrete Res.* 37, 1590–1597. doi: 10.1016/j.cemconres.2007.08.018

Fernández-Jiménez, A., and Palomo, A. (2005). Composition and microstructure of alkali activated fly ash binder: effect of the activator. *Cement Concrete Res.* 35, 1984–1992. doi: 10.1016/j.cemconres.2005.03.003

Gao, X., Yu, Q., and Brouwers, H. (2015). Reaction kinetics, gel character and strength of ambient temperature cured alkali activated slag–fly ash blends. *Construct. Build. Mat.* 80, 105–115. doi: 10.1016/j.conbuildmat.2015.01.065

Garcia-Lodeiro, I., Palomo, A., Fernández-Jiménez, A., and Macphee, D. (2011). Compatibility studies between NASH and CASH gels. study in the ternary diagram Na_2O–CaO–Al_2O_3-SiO_2-H_2O. *Cement Concrete Res.* 41, 923–931. doi: 10.1016/j.cemconres.2011.05.006

Hardjito, D., and Rangan, B. V. (2005). *Development and Properties of low-Calcium Fly Ash-Based Geopolymer Concrete.* CURTIN University of Technology, Research Report. Perth, WA. Available online at: http://hdl.handle.net/20.500.11937/5594

Holt, E. E. (2001). *Early Age Autogenous Shrinkage of Concrete.* Espoo: Technical Research Centre of Finland.

Humad, A. M., Provis, J. L., and Cwirzen, A. (2018). Alkali activation of a high MgO GGBS – fresh and hardened properties. *Magaz. Concrete Res.* 70, 1–24. doi: 10.1680/jmacr.17.00436.

Ismail, I., Bernal, S. A., Provis, J. L., San Nicolas, R., Hamdan, S., and van Deventer, J. S. (2014). Modification of phase evolution in alkali-activated blast furnace slag by the incorporation of fly ash. *Cement Concrete Comp.* 45, 125–135. doi: 10.1016/j.cemconcomp.2013.09.006

Jang, J., Lee, N., and Lee, H. (2014). Fresh and hardened properties of alkali-activated fly ash/slag pastes with superplasticizers. *Construct. Build. Mat.* 50, 169–176. doi: 10.1016/j.conbuildmat.2013.09.048

Keulen, A., van Zomeren, A., and Dijkstra, J. (2018). Leaching of monolithic and granular alkali activated slag-fly ash materials, as a function of the mixture design. *Waste Manage.* 78, 497–508. doi: 10.1016/j.wasman.2018.06.019

Kumar, S., Kumar, R., and Mehrotra, S. (2010). Influence of granulated blast furnace slag on the reaction, structure and properties of fly ash based geopolymer. *J. Mat. Sci.* 45, 607–615. doi: 10.1007/s10853-009-3934-5

Lee, N., Jang, J., and Lee, H. (2014). Shrinkage characteristics of alkali-activated fly ash/slag paste and mortar at early ages. *Cement Concrete Comp.* 53, 239–248. doi: 10.1016/j.cemconcomp.2014.07.007

Lee, N., and Lee, H. (2013). Setting and mechanical properties of alkali-activated fly ash/slag concrete manufactured at room temperature. *Construct. Build. Mat.* 47, 1201–1209. doi: 10.1016/j.conbuildmat.2013.05.107

Lee, N., and Lee, H. (2015). Reactivity and reaction products of alkali-activated, fly ash/slag paste. *Construct. Build. Mat.* 81, 303–312. doi: 10.1016/j.conbuildmat.2015.02.022

Liu, Y., Zhu, W., and Yang, E. (2016). Alkali-activated ground granulated blast-furnace slag incorporating incinerator fly ash as a potential binder. *Construct. Build. Mat.* 112, 1005–1012. doi: 10.1016/j.conbuildmat.2016.02.153

Ma, J., and Dehn, F. (2017). Shrinkage and creep behavior of an alkali-activated slag concrete. *Stru. Concrete* 18, 801–810. doi: 10.1002/suco.201600147

Marjanović, N., Komljenović, M., Baščarević, Z., Nikolić, V., and Petrović, R. (2015). Physical–mechanical and microstructural properties of alkali-activated fly ash–blast furnace slag blends. *Ceramics Int.* 41, 1421–1435. doi: 10.1016/j.ceramint.2014.09.075

Mithun, B., and Narasimhan, M. C. (2014). SELF-cured alkali activated slag concrete mixes-an experimental study. *World Acad. Sci. Eng. Tech.* 8, 477–482. doi: 10.5281/zenodo.1093468

Mosale Vijayakumar, R. (2014). *Evaluating Shrinkage of Fly Ash-Slag Geopolymers*. Dissertation/ master's thesis, Urbana; Champaign, IL: University of Illinois.

Myers, R. J., Bernal, S. A., Gehman, J. D., van Deventer, J. S., and Provis, J. L. (2015). The role of al in cross-linking of alkali-activated slag cements. *J. Am. Ceramic Soc.* 98, 996–1004. doi: 10.1111/jace.13360

Myers, R. J., Bernal, S. A., and Provis, J. L. (2017). Phase diagrams for alkali-activated slag binders. *Cement Concrete Res.* 95, 30–38. doi: 10.1016/j.cemconres.2017.02.006

Myers, R. J., Bernal, S. A., San Nicolas, R., and Provis, J. L. (2013). Generalized structural description of calcium–sodium aluminosilicate hydrate gels: the cross-linked substituted tobermorite model. *Langmuir* 29, 5294–5306. doi: 10.1021/la4000473

Nath, P., and Sarker, P. K. (2014). Effect of GGBFS on setting, workability and early strength properties of fly ash geopolymer concrete cured in ambient condition. *Construc. Build. Mat.* 66, 163–171. doi: 10.1016/j.conbuildmat.2014.05.080

Niknezhad, D., Kamali-Bernard, S., and Mesbah, H. (2017). Self-compacting concretes with supplementary cementitious materials: Shrinkage and cracking tendency. *J. Mat. Civ Eng.* 29:04017033. doi: 10.1061/(ASCE)MT.1943-5533.0001852

Oh, J. E., Monteiro, P. J., Jun, S. S., Choi, S., and Clark, S. M. (2010). The evolution of strength and crystalline phases for alkali-activated ground blast furnace slag and fly ash-based geopolymers. *Cement Concrete Res.* 40, 189–196. doi: 10.1016/j.cemconres.2009.10.010

Provis, J. L. (2014). Geopolymers and other alkali activated materials: why, how, and what? *Mat. Struc.* 47, 11–25. doi: 10.1617/s11527-013-0211-5

Provis, J. L., and van Deventer, J. S. (2014). *Alkali Activated Materials*. State of the Art Report of RILEM TC 224-AAM. Dordrecht: Springer/RILEM. doi: 10.1007/978-94-007-7672-2_4

Richardson, I., Brough, A., Groves, G., and Dobson, C. (1994). The characterization of hardened alkali-activated blast-furnace slag pastes and the nature of the calcium silicate hydrate (CSH) phase. *Cement Concrete Res.* 24, 813–829. doi: 10.1016/0008-8846(94)90002-7

Sakai, E., Miyahara, S., Ohsawa, S., Lee, S., and Daimon, M. (2005). Hydration of fly ash cement. *Cement Concrete Res.* 35, 1135–1140. doi: 10.1016/j.cemconres.2004.09.008

Samson, G., Cyr, M., and Gao, X. X. (2017). Formulation and characterization of blended alkali-activated materials based on flash-calcined metakaolin, fly ash and GGBS. *Construct. Building Mat.* 144, 50–64. doi: 10.1016/j.conbuildmat.2017.03.160

Shi, C., Roy, D., and Krivenko, P. (2006). *Alkali-Activated Cements and Concretes*. New York, NY: CRC Press, Taylor & Francis. doi: 10.4324/9780203390672

Singh, B., Rahman, M., Paswan, R., and Bhattacharyya, S. (2016). Effect of activator concentration on the strength, ITZ and drying shrinkage of fly ash/slag geopolymer concrete. *Construct. Build. Mat.* 118, 171–179. doi: 10.1016/j.conbuildmat.2016.05.008

Škvára, F., Šlosar, J., Bohunek, J., and Marková, A. (2003). "Alkali-activated fly ash geopolymeric materials," in *Proceedings of the 11th International Congress on the Chemistry of Cement* (Durban: Cement and Concrete Institute).

Smith, M., and Osborne, G. (1977). Slag/fly ash cements. *World Cement Tech*. 8, 223–224.

Walkley, B., Rees, G. J., San Nicolas, R., van Deventer, J. S., Hanna, J. V., and Provis, J. L. (2018). New structural model of hydrous sodium aluminosilicate gels and the role of charge-balancing extra-framework al. *J. Phys. Chem. C.* 122, 5673–5685. doi: 10.1021/acs.jpcc.8b00259

Wang, S., and Scrivener, K. L. (1995). Hydration products of alkali activated slag cement. *Cement. Concrete Res.* 25. 561–571. doi: 10.1016/0008-8846(95)00045-E

Wardhono, A., Law, D. W., and Strano, A. (2015). The strength of alkali-activated slag/fly ash mortar blends at ambient temperature. *Proc. Eng.* 125, 650–656. doi: 10.1016/j.proeng.2015.11.095

Yang, M., and Jennings, H. M. (1995). Influence of mixing methods on the microstructure and rheological behavior of cement paste. *Adv. Cement Based Mat.* 2, 70–78.

Zhang, W., Zakaria, M., and Hama, Y. (2013). Influence of aggregate materials characteristics on the drying shrinkage properties of mortar and concrete. *Construct. Build. Mat.* 49, 500–510. doi: 10.1016/j.conbuildmat.2013.08.069

Zheng, Y. C. (2009). *Shrinkage Behaviour of Geopolymer*. Dissertation/master's thesis, Melbourne, VIC: The University of Melbourne.

Conflict of Interest Statement: The authors declare that the research was conducted in the absence of any commercial or financial relationships that could be construed as a potential conflict of interest.